Available online at [www.sciencedirect.com](http://www.sciencedirect.com)

ScienceDirect

[www.elsevier.com/locate/jmbbm](http://www.elsevier.com/locate/jmbbm)

## Research Paper

# An accelerated buoyancy adhesion assay combined with 3-D morphometric analysis for assessing osteoblast adhesion on microgrooved substrata



J.M. Sobral<sup>a</sup>, V.N. Malheiro<sup>b,e</sup>, T.W. Clyne<sup>a</sup>, J. Harris<sup>c,f</sup>, R. Rezak<sup>b</sup>, W. O'Neill<sup>d</sup>, A.E. Markaki<sup>b,\*</sup>

<sup>a</sup>Department of Materials Science & Metallurgy, Cambridge University, 27 Charles Babbage Road, Cambridge CB3 0FS, UK

<sup>b</sup>Department of Engineering, Cambridge University, Trumpington Street, Cambridge CB2 1PZ, UK

<sup>c</sup>Cancer Research UK, Cambridge Research Institute, Robinson Way, Cambridge CB2 9RE, UK

<sup>d</sup>Institute for Manufacturing, Cambridge University, 17 Charles Babbage Road, Cambridge CB3 0FS, UK

<sup>e</sup>EMPA, Swiss Federal Laboratories for Materials Science and Technology, Biointerfaces, Lerchenfeldstrasse 5, 9014 St Gallen, Switzerland

<sup>f</sup>South Glasgow University Hospital, School of Medicine, 1345 Govan Road, Glasgow G51 4TF, UK

## ARTICLE INFO

## Article history:

Received 13 October 2015

Received in revised form

15 December 2015

Accepted 22 December 2015

Available online 1 January 2016

## Keywords:

Cell adhesion

Surface topography

Laser ablation

Centrifugation

## ABSTRACT

An accelerated negative buoyancy method has been developed to assess cell adhesion strength. This method has been used in conjunction with 3-D morphometric analysis to understand the effects of surface topology on cell response. Aligned micro-grooved surface topographies (with a range of groove depths) were produced on stainless steel 316L substrates by laser ablation. An investigation was carried out on the effect of the micro-grooved surface topography on cell adhesion strength, cell and nucleus volumes, cell phenotypic expression and attachment patterns. Increased hydrophobicity and anisotropic wettability was observed on surfaces with deeper grooves. A reduction was noted in cell volume, projected areas and adhesion sites for deeper grooves, linked to lower cell proliferation and differentiation rates and also to reduced adhesion strength. The results suggest that the centrifugation assay combined with three-dimensional cell morphometric analysis has considerable potential for obtaining improved understanding of the cell/substrate interface.

© 2016 The Authors. Published by Elsevier Ltd. This is an open access article under the CC BY license (<http://creativecommons.org/licenses/by/4.0/>).

\*Corresponding author. Tel.: +44 1223 766417.

E-mail address: [am253@cam.ac.uk](mailto:am253@cam.ac.uk) (A.E. Markaki).

## 1. Introduction

Over recent decades, many studies have focused on optimising the interface between implants and surrounding tissue. Failure of prostheses, particularly loosening of the bond with surrounding tissue, is a major concern (McGee et al., 2000). Successful implantation depends critically on how the bond is formed during the initial period of contact. Several methods have been developed to measure cell adhesion strength on grooved surfaces – see review Garcia and Gallant (2003). The tendency towards increased adhesion strength on micro-grooved substrates was corroborated by enzymatic detachment studies (Anselme et al., 2002; Chen et al., 2007; Ismail et al., 2007; Chen et al., 2009). Although these techniques are capable of providing some useful information on cell adhesion, they yield no quantitative information. Furthermore, enzyme activity can be influenced by the nature of the solid/liquid interface (Koutsopoulos et al., 2007), which in turn can be affected by topographic effects.

To quantify cell-substrate adhesion strength, techniques that can provide well-defined mechanical-based parameters are needed. Centrifugation is a simple, reproducible technique that provides reliable quantitative measurements of cell adhesion (McClay et al., 1981; Reyes and García, 2003) by detaching a population of adherent cells through the application of normal or shear stresses. However, the centrifugation assay applies relatively low detachment forces and has therefore been limited to short adhesion times, typically less than 60 min, as at longer adhesion times, cellular attachment strength exceeds the maximum centrifugal force and the assay loses sensitivity (Gallant, 2013).

It is not clear whether cell proliferation and differentiation is intrinsically linked to cell and nucleus morphological characteristics on grooved surfaces. Arguably, cells need to be able to spread in order to enter phase S of the cell cycle during proliferation (Alberts et al., 2002) and if sufficient spreading is not achieved, their proliferation may be inhibited. The addition of topographical features, such as grooves, brings additional physical challenges for cells, probably impeding sufficient spreading essential to achieve normal or improved proliferation rates. Nevertheless, various cell types, such as mesenchymal stem cells (Gerecht et al., 2007), osteoblasts (Kenar et al., 2006; Erdoğan et al., 2011), fibroblasts (Wang et al., 2010) and epithelial cells (den Braber et al., 1996; Khang et al., 2008) have shown to increase their proliferation rates on micro-grooved surfaces. Similarly, regarding osteogenic differentiation, some studies reported increased osteogenic differentiation markers on grooved surfaces (Mata et al., 2009; Lee et al., 2010), while others suggest no significant effects or reduction of cell differentiation (Bruinink and Wintermantel, 2001; Kenar et al., 2006; Holthaus et al., 2012). While the wide range of materials, cell types and experimental conditions again makes it difficult to draw clear universal conclusions, these studies do suggest that the presence of grooves can affect cell morphology, gene expression, proliferation and the strength of adhesion.

Several techniques have been used previously to create well-defined surface topographic features. These include photolithography, electron beam lithography, interference

lithography, soft lithography, casting, grit blasting etc. Although such techniques can create well-defined (nano- and micro-scale) topographic features, most of them do suffer from certain limitations and in some cases they are not well-suited to the range of materials commonly used for implants – i.e. relatively hard metals and ceramics. The use of lasers, on the other hand, introduces considerable versatility, since there is a lot of scope for their accurate control and they can melt/ablate virtually any material. In fact, lasers have already been used for surface topography modification in implants and other biomedical devices (e.g. Duncan et al., 2002; Lawrence et al., 2006; Wang et al., 2008; Qin et al., 2014; Zheng et al., 2015).

In this study, an accelerated-buoyancy adhesion test (up to 112,000 g) in conjunction with 3D morphometric analysis was used on micro-grooved surfaces to measure cell adhesion strength and study topology effects on cell attachment/morphology. Aligned micro-grooved surface topographies with a range of groove depths and fixed width were produced on stainless steel 316L substrates by laser ablation. The use of lasers introduces considerable versatility, since there is a lot of scope for their accurate control and they can melt/ablate virtually any material. Unlike most previous studies, cell adhesion experiments were performed 3 days after seeding, allowing for the cell/substrate contact areas to increase.

## 2. Experimental procedures

### 2.1. Material and sample preparation

Mirror-finish 316L (austenitic) stainless steel sheets, supplied by Aalco (Roundtree Way, Mousehold Lane, Norwich, NR7 8SR, UK), were used for this study. The sheets were 0.9 mm in thickness. Circular discs of 11 mm diameter were cut from these sheets, using a water-jet cutter.

### 2.2. Laser ablation treatment

Samples were surface-treated using a pulsed Ytterbium (Yb) fibre laser, G3 SP-20P-0011, supplied by SPI lasers. Details of the laser system are described elsewhere (O'Neill and Kun, 2009). The laser processing conditions employed are listed in Table 1. Sets of parallel grooves were produced on disc surfaces, as illustrated in Fig. 1. They were designed to generate both relatively coarse undulations and finer scale topographic features. In order to minimise oxidation, laser ablation was carried out using argon as a shrouding atmosphere. Discs polished down to a 0.3 µm finish served as control surfaces. For cell culture studies and material characterisation, the surfaces were cleaned ultrasonically for 5 min, sequentially, in acetone, ethanol, and isopropanol, and then left to dry overnight submerged in ethanol, inside a flow cabinet. Between the acetone and ethanol washing steps, the surfaces were wiped with an ultra-soft cloth (Metprep, UK) soaked in 100% ethanol. After this, the samples were sterilised at 160 °C for 2 h.

**Table 1 – Processing conditions, average groove width and depth and roughness data, obtained using both optical interferometry and atomic force microscopy (AFM) techniques. LT surfaces were laser-treated with an average power of 10 W and a pulse frequency of 125 kHz. No AFM roughness values are shown for LT-22, since the depth was out of the z-range of the equipment. Nomenclature: “LT- $d_g$ ”, where LT stands for laser treated and  $d_g$  is the groove depth.**

Surface	Scanning speed ( $\text{m s}^{-1}$ )	No. of scans	Groove width, $w_g$ ( $\mu\text{m}$ )	Groove depth, $d_g$ ( $\mu\text{m}$ )	Roughness, $R_a$ ( $\mu\text{m}$ ) (45° to the groove long axis)	
					Optical interferometry	AFM
Polished	–	–	–	–	0.004±0.001	0.006±0.001
LT-3.5	1.0	1	40±0.3	3.5±0.32	0.80±0.06	0.76±0.07
LT-7	0.5	1	40±0.2	7.0±0.27	1.67±0.05	1.51±0.03
LT-22	0.5	3	40±0.3	22±0.29	4.74±0.21	

### 2.3. Topographic and chemical characterisation

#### 2.3.1. Atomic force microscopy (AFM)

Topographic features were studied using a Digital Instruments Nanoscope (Veeco Instruments, UK) atomic force microscope. The laser-ablated surfaces were investigated in tapping mode, with silicon nitride tips (Veeco Instruments, UK). Scanning areas were selected according to the type of analysis: (a)  $5 \times 5 \mu\text{m}^2$  for average roughness ( $R_a$ ) measurements and (b)  $100 \times 100 \mu\text{m}^2$  for 3D renderings. Scanning was carried out at 45° to the groove long axis, in order to reduce errors associated with the sharp borders of the grooves. The frequency was slightly adapted, depending on the scanning area and type of surface analysed, but in most cases it was between 0.3 and 0.5 Hz. Two samples of each type were analysed ( $n=2$ ). The cross-sections were characterised in terms of groove depth ( $d_g$ ) and width ( $w_g$ ). The software packages employed were Digital Instruments v.7.30 (Veeco Instruments, UK) and Scanning Probe Imaging Processor (SPIP) (Image Metrology A/S, Denmark).

#### 2.3.2. Interferometric optical profilometry

The surface topography was also investigated using a Veeco Wyko NT3300 Interferometer. A  $20 \times$  objective lens was used. Three scans, with a  $200 \times 200 \mu\text{m}^2$  scan area, were taken randomly from each sample. Four samples of each type were analysed ( $n=4$ ). Surface maps and  $R_a$  measurements were obtained using the Veeco Vision 3.43 and the SPIP imaging softwares (Image Metrology A/S, Denmark).

#### 2.3.3. Contact angle (CA) measurement

Static contact angles were measured using Millipore water ( $R=18 \text{ M}\Omega$ ) with a KSV CAM 200 goniometer (KSV Instruments), using the sessile drop method. A drop was released onto the surface and imaged from the side using a planar CCD camera. Measurements were performed at room temperature, using  $1 \mu\text{L}$  droplets. Photographs of the water drop were taken, after stabilisation (for 5 s), parallel and transverse to the grooves. Six samples were studied for each type ( $n=6$ ) and three measurements were carried out on each sample. The results were analysed using the KSV Instruments software.

### 2.4. Cell culture studies

#### 2.4.1. Sourcing and handling of cells

Primary foetal human osteoblasts (fHOb) were obtained from the European Collection of Cell Cultures (ECCC, UK). Cells were cultured at 37 °C, in a humidified atmosphere containing 5%  $\text{CO}_2$ , using McCoy's 5A medium (Invitrogen, UK), supplemented with 10% of heat-inactivated foetal bovine serum (Invitrogen, UK) and 1% of penicillin–streptomycin (Gibco, USA). Fifth passage cells were used for all cell culture experiments. For osteogenic induction experiments in laser-patterned samples, cells were cultured in an osteogenic medium that consisted of the basic medium supplemented with 10 mM dexamethasone (D4902, Sigma, United Kingdom) and 2 mM  $\beta$ -glycerol phosphate (50020, Sigma, United Kingdom).

#### 2.4.2. Accelerated buoyancy adhesion characterisation test

To quantify the adhesive strength of cells to substrates, buoyancy forces were generated under enhanced acceleration, in a swing-bucket ultra-centrifuge. The procedure is described in detail elsewhere (Robinson et al., 2011). In this study, in order to ensure similar seeding efficiencies between samples, customised holders were designed to hold the specimens inside 24-well plates, leaving only a circular area of 10 mm in diameter available for the cells to attach – see Fig. 2. A total of about 4000 cells were seeded to each sample ( $5093 \text{ cells/cm}^2$ ). This relatively low cell density was chosen so that individual cells were not in contact with their neighbours and showed little or no expression of extracellular matrix. Forces acted normal to the plane of the substrate. The rotational speed was 25,000 rpm and the radial distance of the substrates was approximately 160 mm, generating accelerations of around 112,000 g. The samples were centrifuged for a fixed period of 7 min. Six samples ( $n=6$ ) were used for each specimen type and the tests were performed 3 days after seeding. The proportion of cells remaining adhered to the substrates was estimated by calculating the number of cells before and after centrifuging using the CyQUANT assay (Section 2.4.5).

#### 2.4.3. Scanning electron microscopy (SEM)

Cell morphology was studied using a JEOL 5800LV, with an accelerating voltage of 10 kV and a working distance of about 10 mm. Cell-seeded samples were rinsed twice with warm

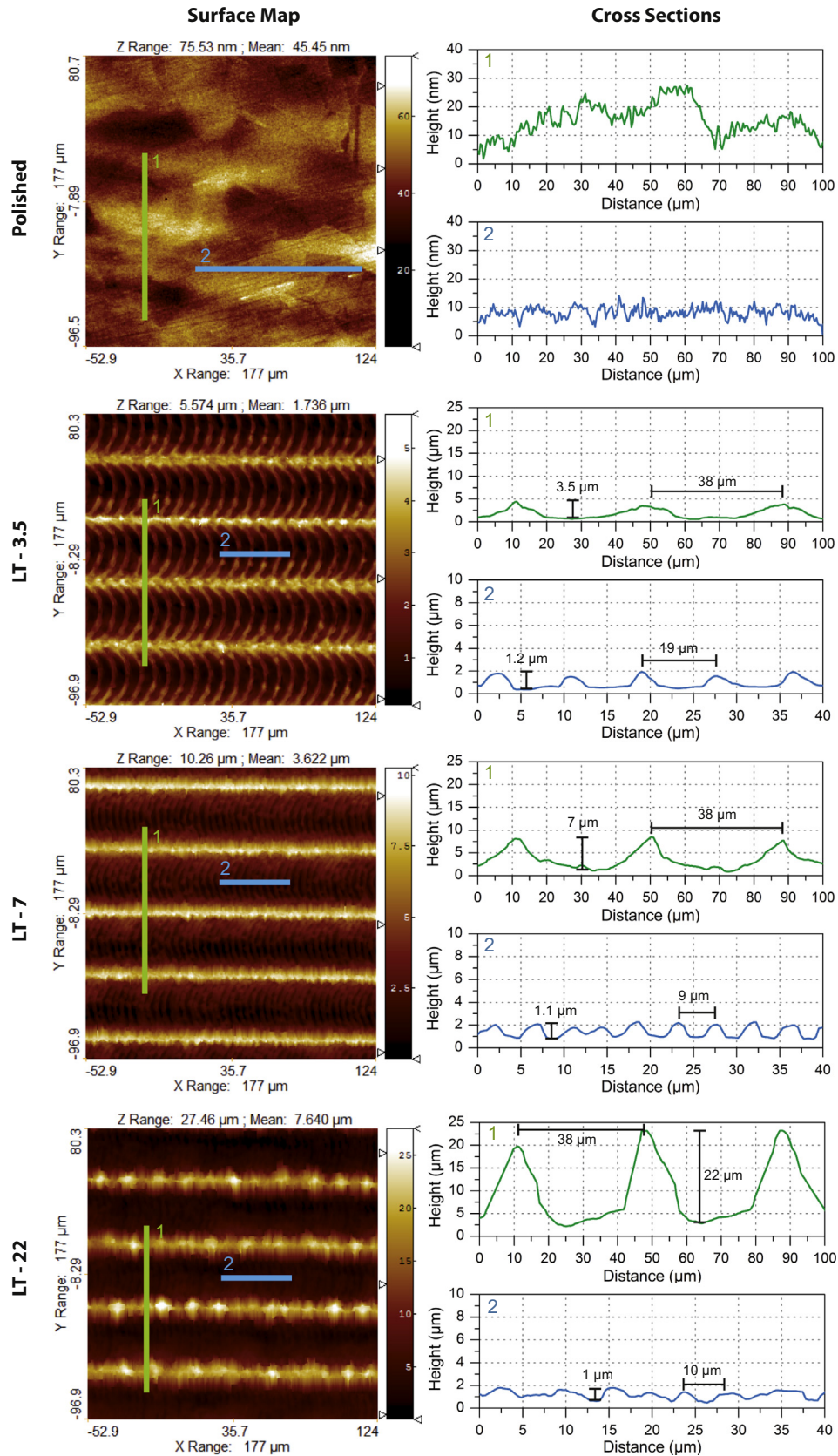
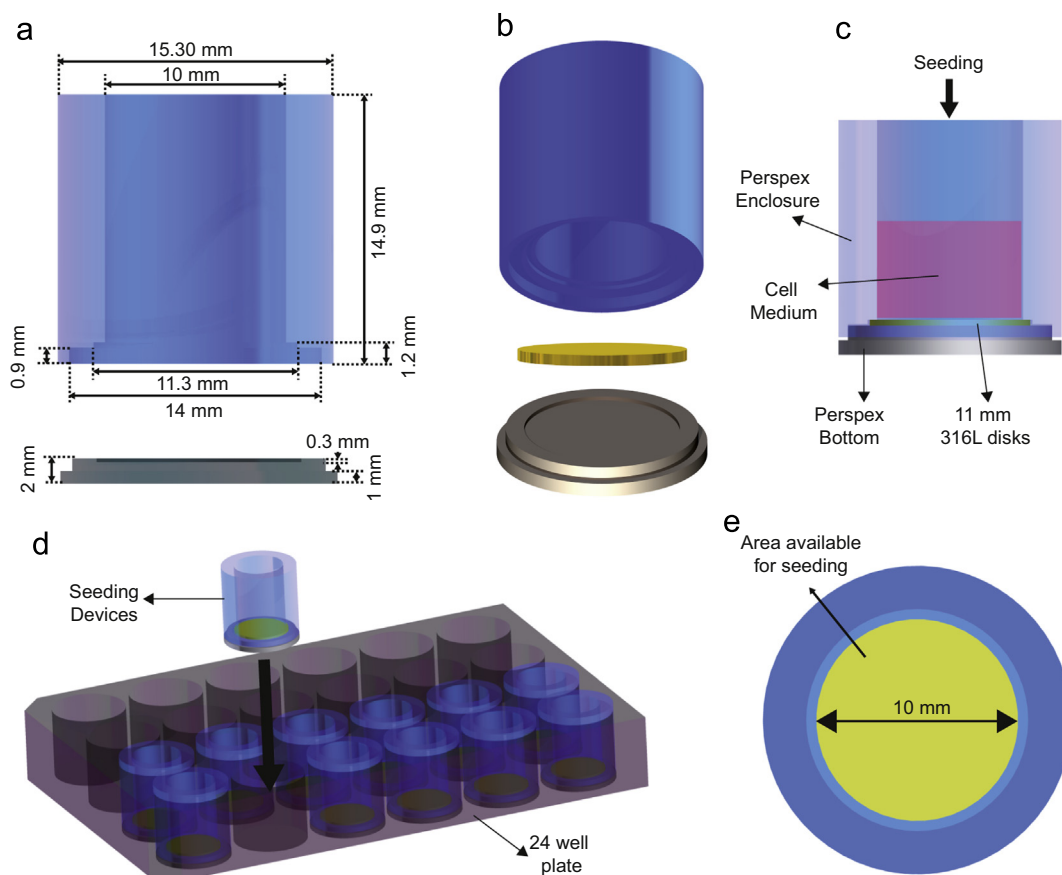


Fig. 1 – Data obtained using interferometric optical profilometry showing 2D surface maps and sectional profiles measured parallel (blue lines) and perpendicular (green lines) to groove direction. (For interpretation of the references to color in this figure, the reader is referred to the web version of this article.)



**Fig. 2** – Schematic showing (a) the dimensions of the top and bottom part of the seeding device, (b) 3D view of the seeding device containing a stainless steel disc (shown in yellow), (c) side view of the seeding device fully assembled with a stainless steel disc, (d) a 24-well plate containing the seeding devices and (e) top view of the seeding device with a sample (yellow) showing the area available for the cells to attach. (For interpretation of the references to color in this figure legend, the reader is referred to the web version of this article.)

buffer solution and placed in a cold 24-well culture plate, with 500  $\mu\text{L}$  of primary fixative (2.5% glutaraldehyde in 0.1 M sodium cacodylate buffer (pH 7.4)). After 1 h, the fixative was removed and the samples were washed twice in PBS. The cells were then dehydrated, by soaking in a series of ethanol solutions (30%, 50%, 70%, 90% and 100%) for 20 min each. Finally, the samples were soaked for 5 min in hexamethyldisilazane (HMDS), before allowing air-drying overnight. Once dry, the discs were attached to SEM stubs with double-sided carbon tape and then sputter-coated with Pt for 2 min at 40 keV.

#### 2.4.4. Confocal laser scanning microscopy (CLSM)

After 3 days in culture, the cells were fixed in 4% paraformaldehyde/phosphate buffer solution (PBS), with 1% sucrose, for 15 min at room temperature. The cell-seeded samples were then washed with PBS and permeabilised in 0.15% Triton® X-100 (Sigma, UK) in PBS for 15 min at room temperature. Samples were then subjected to the following immuno-labelling protocols.

**2.4.4.1. 2D and 3D morphometric analysis.** Samples were incubated in the dark in FITC conjugated phalloidin (P5282,

Sigma, UK) at  $5 \mu\text{g mL}^{-1}$  (1:100 in 1% BSA/PBS, Sigma, UK) for 40 min at 37 °C. They were then washed and incubated in the dark with 2  $\mu\text{g/mL}$  HCS CellMask red cytoplasmic/nuclear stain (H32711, Invitrogen, UK) in PBS for 30 min at room temperature. Samples were then washed twice with PBS before mounting on the Vectorshield fluorescent mountant containing DAPI for nuclear labelling (Vector Laboratories, UK). Approximately 100–150 individual cells per type were analysed using the Volocity 5.5.1 software (PerkinElmer, USA). 2D and 3D image z-stacks were acquired with a Nikon 20 $\times$ /0.75 N.A. Plan Fluor Multi-Immersion lens. The channels for DAPI, FTIC conjugated phalloidin and HCS were merged using a brightest point algorithm. All cells and nuclei were automatically identified, thresholded and reconstructed in the merged channel using Volocity standard measurement protocols. The area and orientation of cells and nuclei were obtained using CLSM images – see Fig. A.1 (Appendix). A box was fitted to each cell/nucleus using the Volocity software and the diagonal overlapping the cell/nucleus was traced. The cell orientation was obtained from the angle between the traced diagonal and the groove long axis (laser-patterned samples) or a random line (polished surfaces). The nucleus elongation factor was the ratio of the shortest axis of the

nucleus to its longest. Fig. A.2 shows typical CLSM images, and 3D reconstructions used for obtaining cell and nuclei volumes.

**2.4.4.2. Focal adhesion analysis.** Samples were incubated in 1% BSA in PBS for 30 min at room temperature, to block unspecific binding sites of antibodies. They were then incubated at room temperature (in the dark) for 1.5 h in 1:150 primary antibody monoclonal Anti-Vinculin antibody in 1% BSA/PBS (V9131, Sigma, UK). Anti-vinculin labelling (orange) was used to detect the adhesions. Once this step was complete, the samples were rinsed three times with PBS containing 0.05% of Tween® 20 (P2287, Sigma, UK) and then incubated in 1:200 AlexaFluor 594 goat anti-mouse secondary antibody in 1% BSA/PBS (A11005, Invitrogen, UK) for 1 h at room temperature (in the dark). After washing the samples three times with PBS containing 0.05% of Tween® 20, they were incubated in the dark in FITC conjugated phalloidin (P5282, Sigma, UK) at  $5 \mu\text{g mL}^{-1}$  (1:100 in 1% BSA/PBS, Sigma, UK) for 40 min at  $37^\circ\text{C}$ . Samples were washed twice with PBS, before mounting on the Vectorshield fluorescent mountant containing DAPI for nuclear labelling. The Volocity software was used to automatically find and analyse adhesion sites. 3D image z-stacks were acquired using a Nikon  $60\times/1.3$  N.A. Plan Apo VC Oil Immersion lens. The adhesion frequency was calculated as the mean number of adhesions per cell. The criteria for adhesion classification were taken from Bershadsky et al. (2006), where adhesions in the range  $0.5\text{--}2 \mu\text{m}$  are designated as focal complexes (FXs), adhesions between  $2$  and  $5 \mu\text{m}$  as focal adhesions (FAs) and adhesions larger than  $5 \mu\text{m}$  as super-mature adhesions (SMAs). This analysis was combined with the FITC phalloidin and DAPI channels to qualitatively describe the relative position of the adhesion sites according to the morphology of the cell, configuration of the actin filaments and surface topography. About 10–15 cells were tested for each type of surface topography.

Samples were imaged using a Nikon C1 scanning confocal system, with an upright microscope (Nikon Instruments Europe). A UV diode laser, argon ion laser and a red diode laser were used to provide excitation for the chosen fluorophores at wavelengths of 405, 488 and 633 nm respectively. The emission signal produced by each fluorophore upon excitation was collected on separate photo-multiplier tube detectors. To prevent spectral cross-talk between emission signals, a sequential scan mode was employed. All images were acquired using an XY scan resolution of  $1024\times 1024$  pixels, which provided scan areas of  $1.24$  and  $0.414 \text{ mm}^2$ , whilst using the  $20\times$  and  $60\times$  objective lenses respectively. The smallest pinhole setting allowable on the system was used for scanning through the sample in Z. A suitable Z-step size was employed to satisfy the Nyquist sampling theorem for both objective lenses.

#### 2.4.5. Cell proliferation

Cell proliferation was assessed using the CyQUANT Cell Proliferation Assay (Invitrogen, UK). At each time point (1, 4, 7, 10, 15 and 21 days), the medium was aspirated and six samples ( $n=6$ ) from each type were frozen at  $-80^\circ\text{C}$  until required for measurement. After thawing, a CyQUANT lysis

buffer was added to each sample and the solution was agitated. A volume of  $50 \mu\text{L}$  of the cell lysate was transferred to a black 96-well plate and  $50 \mu\text{L}$  of the CyQUANT dye was added. DNA content was measured fluorimetrically (excitation  $480 \text{ nm}$ , emission  $520 \text{ nm}$ ), using a BMG Labtech FLUOstar Optima plate reader. Fluorescence readings were converted to cell numbers through a standard curve. For this, a range of cell concentrations were seeded onto 24-well plates and prepared in the same manner as the samples. Cells were seeded at a density of 10,000 cells per sample ( $\sim 12,732 \text{ cells cm}^{-2}$ ). To prevent cell growth, the cells were frozen 24 h after seeding.

#### 2.4.6. Cell differentiation

Alkaline phosphatase (ALP) enzymatic activity was used as a marker for early osteoblastic differentiation, using 6,8-difluoro-4-methylumbelliferyl phosphate (DiFMUP) as a fluorogenic substrate. The reaction of ALP with DiFMUP can be followed at  $358 \text{ nm}$ , as 6,8-difluoro-7-hydroxy-4-methylcoumarin (DiFMU) is produced. ALP activity was assessed fluorimetrically, following the mixing  $50 \mu\text{L}$  of the cell lysate prepared for the CyQUANT assay with  $50 \mu\text{L}$  ALP assay buffer containing DiFMUP and incubating at  $37^\circ\text{C}$  for 15 min in the absence of light. The reaction was measured twice in each sample. The releasing fluorescent DiFMU was measured using a BMG Labtech FLUOstar Optima plate reader at  $358 \text{ nm}$  excitation and  $455 \text{ nm}$  emission. The signal was measured in fluorescence emission intensity units and converted to quantity of DiFMU produced, using a DiFMU standard curve. This experiment was performed on the same samples used for the proliferation analysis ( $n=6$ ).

#### 2.4.7. Statistical analysis

For cell adhesion experiments, averages of two independent studies, with six replicates per surface, were expressed as the arithmetic mean  $\pm$  SD. For cell proliferation and differentiation, three independent experiments, with six replicates per surface, were conducted. Results are presented and expressed as the arithmetic  $\pm$  standard deviation (SD). Data were analysed using Tukey analysis of variance (ANOVA), with Graphpad Prism software (Graphpad Software Inc., USA). Differences were considered statistically significant at  $p$  values of  $<0.05$ .

## 3. Surface characterisation

### 3.1. Surface topography

3D surface maps and section profiles, obtained using optical interferometry, are shown in Fig. 1. Section profiles were taken parallel (blue lines) and perpendicular (green lines) to the groove direction. Table 1 lists the laser processing conditions employed to produce micro-grooved surfaces, the groove dimensions (depth ( $d_g$ ) and width ( $w_g$ )) and the average surface roughness,  $R_a$ . While the polished surface is featureless and flat, the laser treated (LT) surfaces exhibit parallel grooves, containing a series of sub-micron “lips” ( $\sim 1.1 \mu\text{m}$  – see Fig. 1) within. These “lips” are produced by surface melting and refreezing phenomena associated with

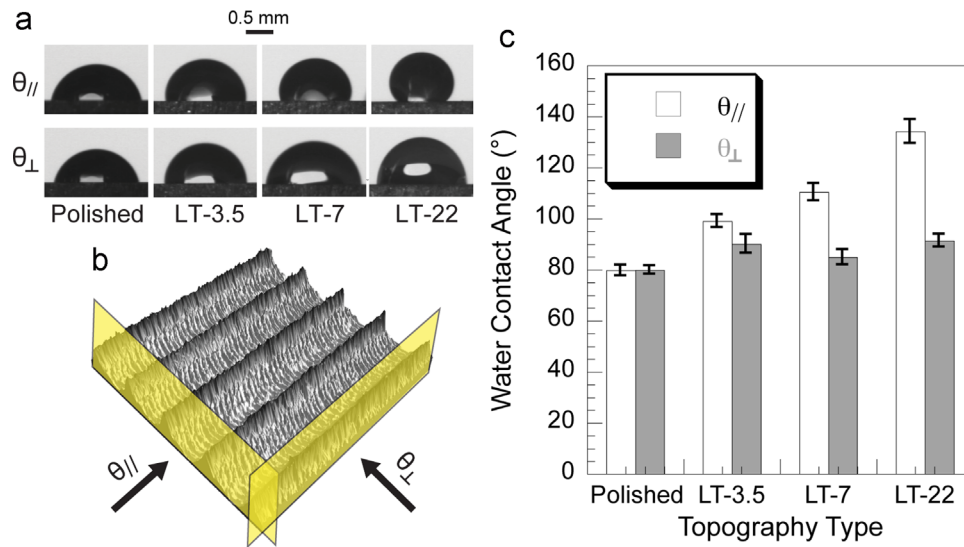


**Fig. 3 – (a) Optical micrographs of 1  $\mu$ L water droplets on polished and micro-grooved surfaces. On the patterned surfaces, measurements were made parallel ( $\theta_{//}$ ) and perpendicular ( $\theta_{\perp}$ ) to the long axis of the grooves; (b) schematic representation of a water droplet on a micro-grooved surface; (c) water contact angle measurements.**

individual laser pulses (Kurella and Dahotre, 2005). The spacing between these lips, and also the groove depth, are determined by the scanning speed and the number of irradiation steps (i.e. the number of repeated scans in the same area). All patterns have the same groove width ( $\sim 40 \mu\text{m}$ ), since the laser beam spot size was fixed, but varied in groove depth (Table 1). The LT surfaces are designated, on the basis of their groove depth, “3.5  $\mu\text{m}$ ”, “7  $\mu\text{m}$ ” and “22  $\mu\text{m}$ ”.  $R_a$  values (Table 1), taken at  $45^\circ$  to the groove long axis, increase from a small fraction of a micron ( $\sim 50 \text{ nm}$  – polished surface) to about  $5 \mu\text{m}$  (LT-22 surface). This increase is attributed to the increasing groove depth, whereas the section profiles (blue lines of Fig. 1) show that the roughness of the bottom of the grooves is very similar for all LT surfaces.

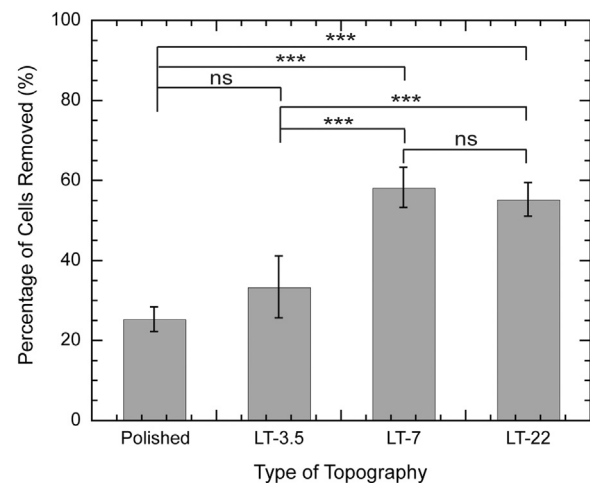
### 3.2. Wetting characteristics

Fig. 3 shows the water drop contact angles measured perpendicular ( $\theta_{\perp}$ ) and parallel ( $\theta_{//}$ ) to the axis of the grooves. Also shown are images of the  $1 \mu\text{L}$  water droplets, taken along both directions. It can be seen that the contact angles measured parallel ( $\theta_{//}$ ) to the groove axis increase with groove depth from  $\sim 80^\circ$  (slightly hydrophilic) on polished surfaces to  $\sim 134^\circ$  (strongly hydrophobic) on LT-22 surfaces. These angles were higher than the corresponding ones measured perpendicular to the groove axis, suggesting a wetting anisotropy for the laser-treated surfaces.

## 4. Cell response

### 4.1. Cell adhesion

The results from the accelerated buoyancy adhesion characterisation test are shown in Fig. 4, as cell removal fractions after centrifuging. It can be seen that the proportion of removed cells is significantly higher on the laser-treated



**Fig. 4 – Percentage of cells removed after centrifuging, using an acceleration of 112,000 g. The tests were performed 3 days after seeding and cell numbers were measured using the CyQUANT assay. (Mean  $\pm$  SD; ns – non-significant; \*\*\* $p < 0.001$ ).**

samples with deeper grooves (LT-7 and LT-22) compared to polished or shallow-grooved samples (LT-3.5). No significant differences were detected between the LT-7 and LT-22 surfaces, and also between the polished and LT-3.5 surfaces.

### 4.2. Cell morphology

Fig. 5 shows cell morphologies after 4 days in culture, as obtained by SEM and CLSM. It can be seen that, on the polished surfaces, cells exhibit a polygonal morphology typical of an osteoblast in culture. On the laser-treated surfaces, some differences in the attachment pattern were observed between different groove depths. On the LT-3.5 surface, the cell attachment

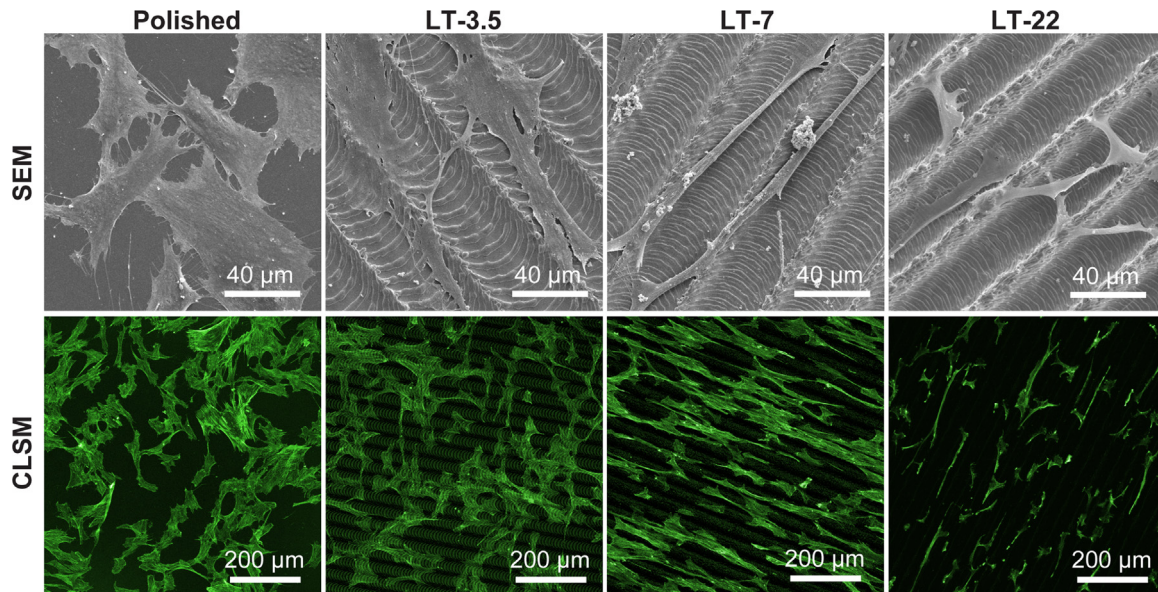


**Fig. 5 – SEM and CLSM images of hFOBs after 4 days in culture on polished and laser-ablated surfaces. CLSM images: Green = Actin. (For interpretation of the references to color in this figure legend, the reader is referred to the web version of this article.)**

pattern was similar to that observed on the polished surfaces. Cells commonly straddled two or more parallel grooves, residing inside the grooves. On the LT-7 and LT-22 surfaces, on the other hand, the majority of cells were elongated in the direction of the groove axis. Cells were bridging the grooves and on the LT-22 surfaces often did not conform to the concave shape of the underlying grooves.

#### 4.3. 2D and 3D morphometric analysis

Cell areas and orientation angles are presented in Fig. 6 (a) and (b) respectively. It can be seen that the LT-7 and LT-22 surfaces exhibit lower projected areas compared to polished and LT-3.5 surfaces (Fig. 6(a)). Cell orientation measurements (Fig. 6(b)) were categorized into 9 bins of  $10^\circ$ . On polished surfaces, no preferred orientation was observed. On LT-3.5 surfaces, a very small proportion of cells exhibit intermediate orientation angles ( $30^\circ$ – $60^\circ$ ) with respect to the groove long axis. The majority of cells are oriented either perpendicular ( $70^\circ$ – $90^\circ$ ) or parallel ( $0^\circ$ – $30^\circ$ ) to the groove direction. On LT-7 surfaces, most hFOBs ( $\approx 40\%$ ) were oriented between  $0^\circ$  and  $40^\circ$ , with the largest proportion of cells found in the  $0^\circ$ – $10^\circ$  group. On sample LT-22 surfaces, the vast majority of hFOBs ( $\approx 30\%$ ) were found in the  $0^\circ$ – $10^\circ$  group.

Nucleus areas and elongation factors are shown in Fig. 6 (c) and (d) respectively. It can be seen that the nucleus area becomes statistically smaller with increasing groove depth. On both LT-7 and LT-22 surfaces, the nucleus is more elongated compared to polished and LT-3.5 surfaces.

Fig. 7 shows typical 3D images of individual hFOBs attached onto the different surfaces. It can be seen that LT-7 surfaces seem to promote a highly elongated morphology, compared with the other two laser-ablated surfaces. The results from the volumetric analysis of cells and nuclei are

shown in Fig. 8. No statistically significant differences ( $p > 0.05$ ) were observed between polished and LT-3.5 surfaces. However, significantly lower cell and nuclei volumes were measured on the LT-22 surfaces, compared with polished and LT-3.5 surfaces.

#### 4.4. Focal adhesions

Quantification of the focal adhesion sites for each surface topography, and type of adhesion (FX, FA or SMA), is presented in Fig. 9(a). It can be seen that the total number of focal adhesion sites, and also the number of focal adhesion sites per type, were lower on the laser-ablated surfaces, compared to polished surfaces. Focal complexes (FXs) and focal adhesions (FAs) were the mostly prominent adhesions. Fig. 9(b) shows correlations between the number of adhesion sites per cell and groove depth.

#### 4.5. Cell proliferation and differentiation

Fig. 10(a) and (b) show respectively cell proliferation and ALP expression on the different surfaces, after 1, 4, 9, 14 and 21 days of culture. Statistical markers are omitted in Fig. 9(a), to promote readability. However, all time points and conditions where standard deviations are not overlapping can be considered statistically significant ( $p < 0.01$ ). It can be seen that polished surfaces exhibit higher cell proliferation rates than laser-ablated surfaces until day 9. From day 9 onwards, on all surfaces, except LT-22, a decrease in proliferation rate was observed as the surfaces started to reach confluence. After day 14, a plateau was reached. Cell numbers were lower on grooved surfaces compared to polished, with numbers decreasing with groove depth until about day 12, after which no effect of groove depth was observed. The ALP activity of the osteoblasts cultured on the different surfaces (Fig. 10(b))

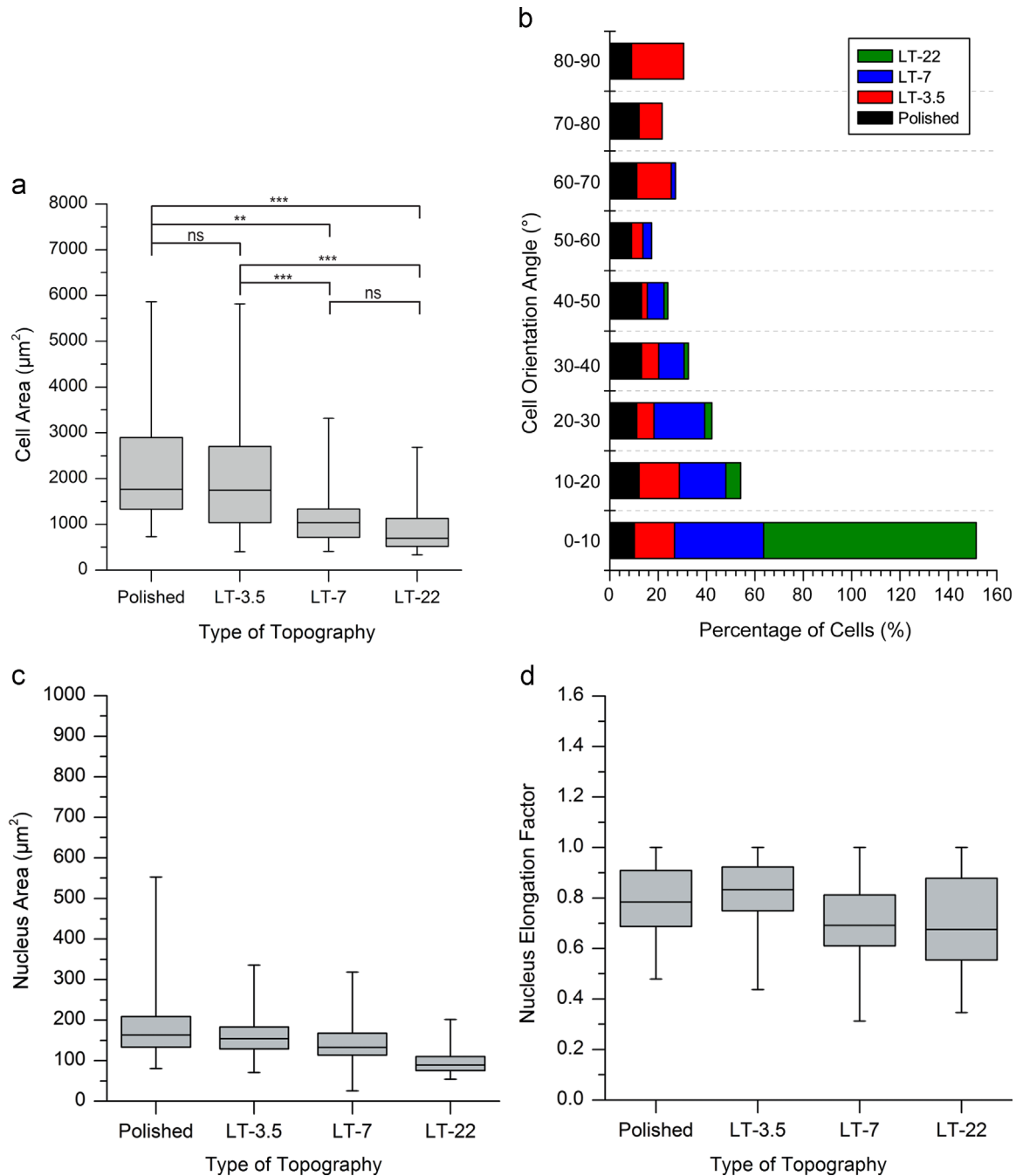


**Fig. 6 – (a) Cell areas and (b) orientation angles (divided into 9 equal bins of 10°), (c) nucleus area and (d) nucleus elongation factor for fHOb cells attached to polished and laser-ablated surfaces after 3 days in culture. In (a), (c) and (d), the values represent minimum, 25th percentile, median, 75th percentile and maximum magnitudes (ns – non-significant; \* $p < 0.05$ , \*\* $p < 0.01$  and \*\*\* $p < 0.001$ ).**

shows that statistically significant differences were only observed from day 9 onwards, with polished surfaces showing higher ALP activity when compared to grooved surfaces.

## 5. Discussion

In this study, an accelerated-buoyancy adhesion test is used, in conjunction with 3D morphometric analysis, to assess cell

adhesion strength and topology effects on cell attachment and morphology. A laser ablation technique was employed to generate micro-grooves on austenitic stainless steel 316L surfaces. To ensure that the effect of surface topology is truly distinguished from that of surface chemistry, XPS analysis was carried out (Fig. A.3 – Appendix). No differences in surface chemistry between laser-ablated and polished surfaces were detected suggesting that any differences in cell response are likely to be attributed to surface topology

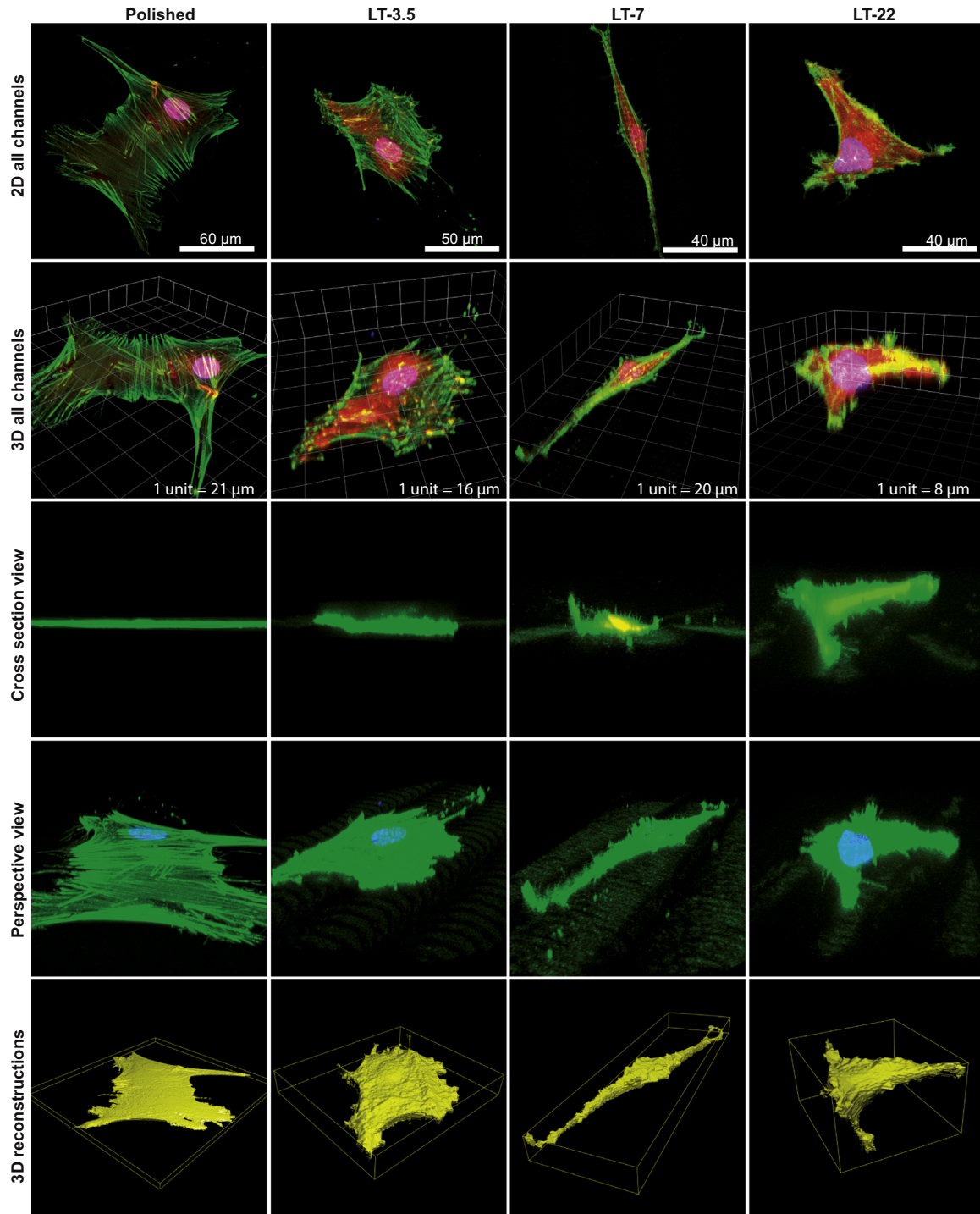


**Fig. 7** – CLSM images and reconstructions of fHObS attached on polished and laser treated 316L surfaces. Red = cell cytoplasm, Green = actin and Blue or Pink = nucleus. The actin channel was saturated in cross sectional and perspective views, so that the micron-scale grooves could be visualised. (For interpretation of the references to color in this figure legend, the reader is referred to the web version of this article.)

effects. Static water contact angle measurements, using drop sizes significantly larger than the groove width (~30 times larger), suggest that the contact angles on the grooved surfaces are higher compared to the polished (isotropic) surface. Additionally, differential elongation of the water droplets was observed on the grooved surfaces. At high

groove depths (LT-7 and LT-22), higher contact angles were measured in the direction parallel to the groove axis ( $\theta_{//}$ ) compared to those measured perpendicular ( $\theta_{\perp}$ ), which is consistent with previous observations on sub- and micron-scale grooved substrates (e.g. Zhao et al., 2007; Ma et al., 2013; Fischer et al., 2014; Kubiak and Mathia, 2014). Spreading

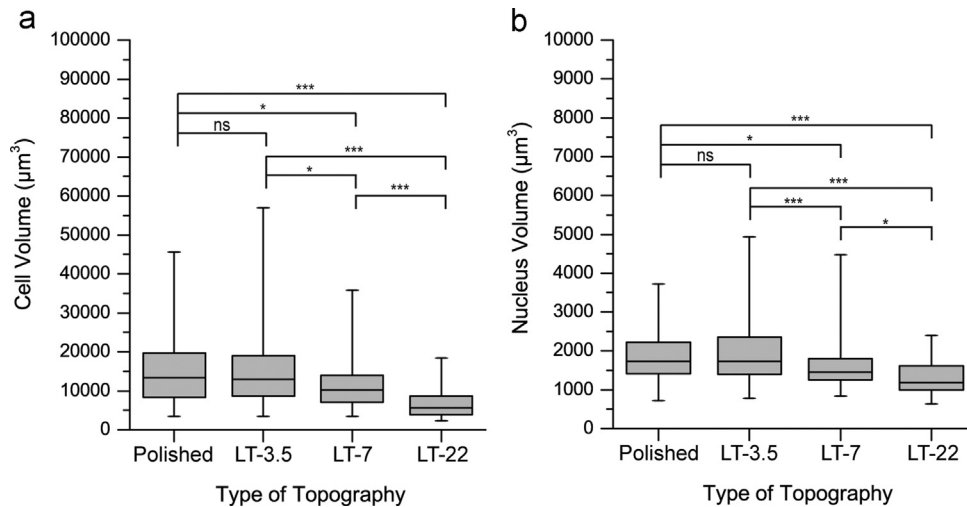


**Fig. 8 – Cell and nucleus volumetric data for fHOBs attached to polished and laser-ablated surfaces after 3 days in culture. The values represent minimum, 25th percentile, median, 75th percentile and maximum magnitudes (ns – non-significant; \* $p < 0.05$ , \*\* $p < 0.01$  and \*\*\* $p < 0.001$ ).**

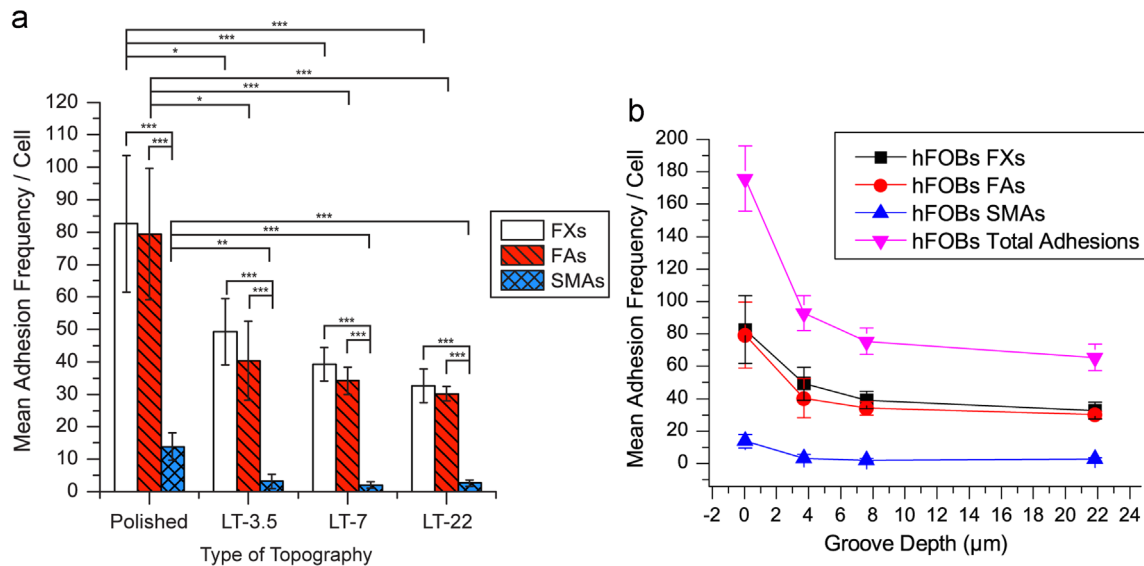


**Fig. 9 – (a) fHOB adhesion types (FX, FA, SMA) on polished and laser-treated surfaces. Data were obtained using an automatic detection algorithm on Volocity (PerkinElmer, USA) using immuno-labelling images of cells stained for vinculin 3 days after seeding. (Mean  $\pm$  SD; \* $p < 0.05$ , \*\* $p < 0.01$  and \*\*\* $p < 0.001$ ). (b) Correlation between adhesion type mean frequency per cell and groove depth.**

orthogonal to the groove decreased with groove depth, whereas along the grooves, spreading was somewhat similar. This suggests that, at high groove depths, the fluid cannot occupy all the available surface area resulting in an increase in the contact angle (higher hydrophobicity). A similar anisotropic wetting behaviour, associated with groove depths, has been reported previously (Zhao et al., 2007) which was attributed to an increasing energy barrier. The wetting state of the water droplet is mainly Wenzel, in which the droplet reaches the bottom surface of the grooves – see e.g. Belaud et al. (2015) for the different wetting regimes. On the LT-22 surface though, the surface is hydrophobic ( $\theta_{//} \sim 134^\circ$ ) and the drop resides mostly on the top of the surface grooves (i.e. the drop does not advance much down on the vertical walls

of the groove) suggesting that the wetting mode is Cassie-Baxter.

No significant differences in cell morphology were detected between polished surfaces and surfaces containing shallow grooves (LT-3.5). On surfaces with deeper grooves (LT-7 and LT-22), on the other hand, a contact guidance effect was observed. The suggestion that deeper grooves (up to 25  $\mu\text{m}$ ) can be more effective in guiding cell orientation is in agreement with previous studies (Clark et al., 1990; Chehroudi et al., 1992; Curtis and Wilkinson, 1997). Fig. 6 (a) shows that the projected cell areas on these surfaces are lower than those on polished and LT-3.5 surfaces, which are more hydrophilic, in agreement with a previous study (Liu et al., 2007). This observation corroborates previous findings

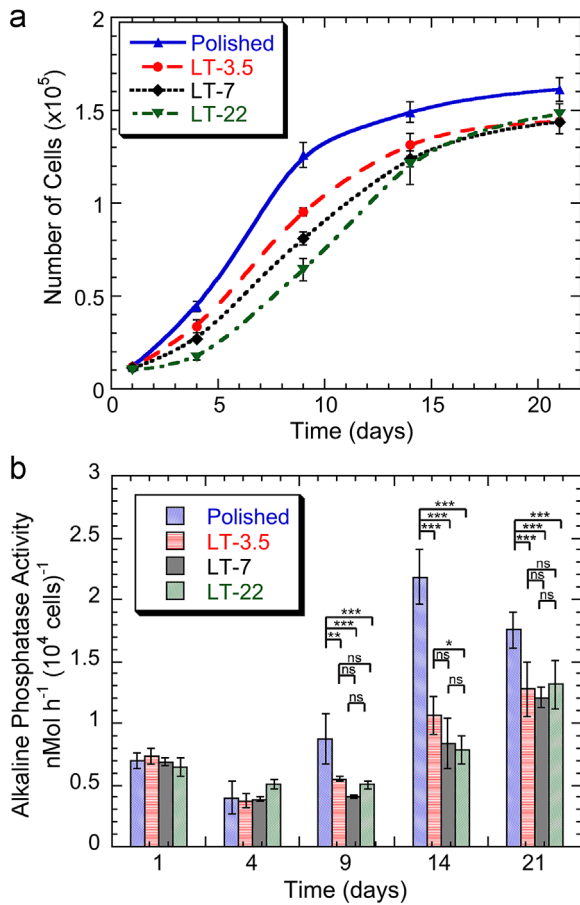


**Fig. 10 – (a) Cell proliferation and (b) alkaline phosphatase (ALP) activity of osteoblasts cultured on the different surfaces, as measured by the CyQUANT assay. Data are presented as the mean  $\pm$  SD. For (b): ns – non-significant; \* $p < 0.05$ , \*\* $p < 0.01$  and \*\*\* $p < 0.001$ .**

(Anselme and Bigerelle, 2005) in which human osteoblasts were found to spread more on surfaces with low roughness than on rough ones. Cell orientation measurements depicted in Fig. 6(b) show that on polished and LT-3.5 surfaces there is no preferred orientation, whereas on the LT-7 and LT-22 surfaces, cells tend to align along the long axis of the groove, which is in agreement with SEM and CLSM observations. Nuclei exhibited lower projected areas and higher elongation factors on deeper micro-grooved surfaces as shown in Fig. 6 (c) and (d) respectively. Cell and nucleus elongation with increasing groove depth has been reported previously on nano-scale grooves (Davidson et al., 2010, 2015).

SEM observations suggest that cells tend to reside within the grooves on LT-3.5 mm surfaces, but on deeper grooves (LT-7 and LT-22), cells often attached to the groove rims and spread from one rim to another, bridging the groove. Bridging is more likely to occur on surfaces with deeper grooves. Osteoblast bridging onto micro-grooved surfaces has been reported previously (Jayaraman et al., 2004; Cao et al., 2009).

Immunolabeling of focal adhesions suggests that fewer adhesion sites per cell were observed on grooved substrates. Focal complexes (FXs) and focal adhesions (FAs) were the

mostly prominent types of adhesion cite. The distribution of adhesion sites exhibits a peak between 1.5 and 2  $\mu\text{m}$  adhesion lengths, which is in agreement with Biggs et al. (2007, 2008a, 2008b and 2009) despite the fact that in these studies quantification of adhesion sites was carried out using 2D images. The total number of focal adhesion sites, and the number of focal adhesion sites per type, was lower on the laser-ablated surfaces, particularly on the LT-7 and LT-22 surfaces, compared to polished surfaces. These surfaces exhibited the lowest cell projected areas. 3D images of fHOb attached onto the different surfaces show elongated stress actin fibres on the deeper grooved surfaces (LT-7 and LT-22). This is particularly evident on the LT-7 surface. Analyses of cell and nucleus volumes show that both decrease when attached to deeper grooves. These volumetric changes suggest that cells adapt their morphology depending on surface topography.

Grooves reduced both fHOb proliferation and early osteogenic differentiation. Jiang et al. (2012) reported a similar result on 0.3  $\mu\text{m}$  deep, U-shape microgrooves (12 and 40  $\mu\text{m}$  wide) seeded with osteoblasts. However, other studies have reported an increase in osteoblast differentiation, (e.g. U-shape microgrooves 0.5–1.5  $\mu\text{m}$  deep, 1–10  $\mu\text{m}$  wide (Matsuzaka et al., 1999), pyramic microgrooves 23  $\mu\text{m}$  deep, 33  $\mu\text{m}$  square base (Jiang et al., 2012), V-shape microgrooves (3, 10, and 30  $\mu\text{m}$  deep and 42  $\mu\text{m}$  wide) (Perizzolo et al., 2001). In the present study, osteoblasts were found to proliferate at a lower rate on the grooved surfaces, compared to polished surfaces. Cell numbers were lower on the grooved surfaces, with numbers decreasing with groove depth before the cells reach confluence. Differences in ALP activity between polished and grooved substrates became statistically significant at day 9, with higher ALP activity on polished surfaces. A peak, denoting the beginning of cell differentiation on the polished surfaces, was observed on day 14, which is consistent with earlier work (Malheiro et al., 2011) on these surfaces.

An accelerated buoyancy technique with customised seeding devices was used to quantify the osteoblast adhesion strength on the different surfaces. The experimental results suggest that osteoblasts adhere stronger on the polished and LT-3.5 surfaces compared to the deeper/more hydrophobic LT-7.5 and LT-22 surfaces. This is consistent with the lower number of adhesion sites (& projected areas) observed for these cases. LT-7 and LT-22 surfaces had similar percentage of cells detached after centrifuging ( $\approx 59\%$ ). Furthermore, one would expect that if cells bridge the grooves they won't take full advantage of the surface area available on the bottom and side of the grooves resulting in reduction of cell adhesion sites. A small reduction of cell adhesion sites was observed between the LT-7 and LT-22 surfaces, which may explain why a similar number of cells were detached from the surfaces after centrifugation. Our study corroborates previous findings (Bigerelle et al., 2002; Anselme and Bigerelle, 2005) on cell adhesion. In these studies, cells were found to adhere better on surfaces with low order.

## 6. Conclusions

In this study, an accelerated buoyancy technique was used to assess how strongly foetal human osteoblast cells attach on stainless steel substrates, with and without sets of parallel grooves (created by laser processing, which left the surface chemistry largely unaffected). Three-dimensional cell morphometric analysis was used to evaluate the effect of surface topography on cell attachment. A reduction was noted in cell and nucleus volume, and cell adhesion strength on grooved, more hydrophobic surfaces, particularly with deep grooves. This is consistent with the lower number of adhesion sites and projected cell areas observed for these cases.

## Acknowledgements

Financial support for this work has been provided by the Engineering and Physical Sciences Research Council (EPSRC, United Kingdom, Grant GR/R95364/01) and by the European Research Council (ERC, Grant No. 240446). The authors are grateful to Dr. Tim Nunney, of Thermo-Fisher Scientific, for carrying out the XPS measurements.

## Appendix

### Experimental details

#### X-ray photoelectron spectroscopy (XPS)

The XPS data were acquired using a Thermo Scientific K-Alpha instrument (Thermo Fisher Scientific, UK), with a base

pressure in the analysis chamber of  $5 \times 10^{-9}$  mbar. The source of radiation was a monochromated Al-Ka X-ray gun (1486.7 eV), operated at a voltage of 12 kV with an emission current of 1.16 mA and a 200  $\mu\text{m}$  X-ray spot. For depth profiling, an  $\text{Ar}^+$  ion gun was used, with a 500 eV ion energy, 1  $\mu\text{A}$  current and an etch rate  $0.21 \text{ nm s}^{-1}$  (based on a calibration on a known  $\text{Ta}_2\text{O}_5$  standard). During depth profiling, the system base pressure was  $8 \times 10^{-8}$  mbar. Compucentric rotation was used during the etch cycle. Data were collected using rapid snapshot acquisition (128 channels, 2 s per element, 150 eV pass energy) and processed using the Thermo Scientific Avantage software.

## Results

### Surface chemistry

Typical XPS depth profiles for as-received and laser-ablated surfaces are shown in Fig. A.3. The profiles are complicated by the presence of a carbonaceous contamination layer, which is inevitably present on the surface, and also by the fact the laser-treated surface is not flat on the scale of the lateral resolution of the XPS. Nevertheless, it can be seen that the chemical composition at the surface is very similar for as-received and laser-ablated surfaces. The depth profiles suggest a thicker oxide layer on the laser-treated surfaces, which is unsurprising.

See Figs. A.1–A.3.

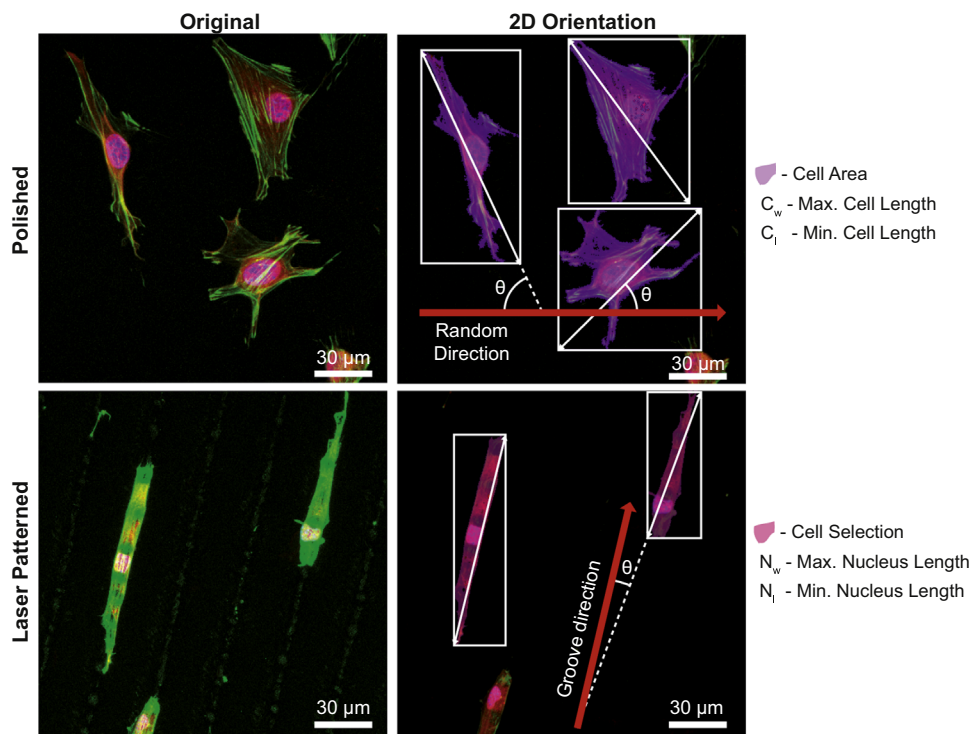
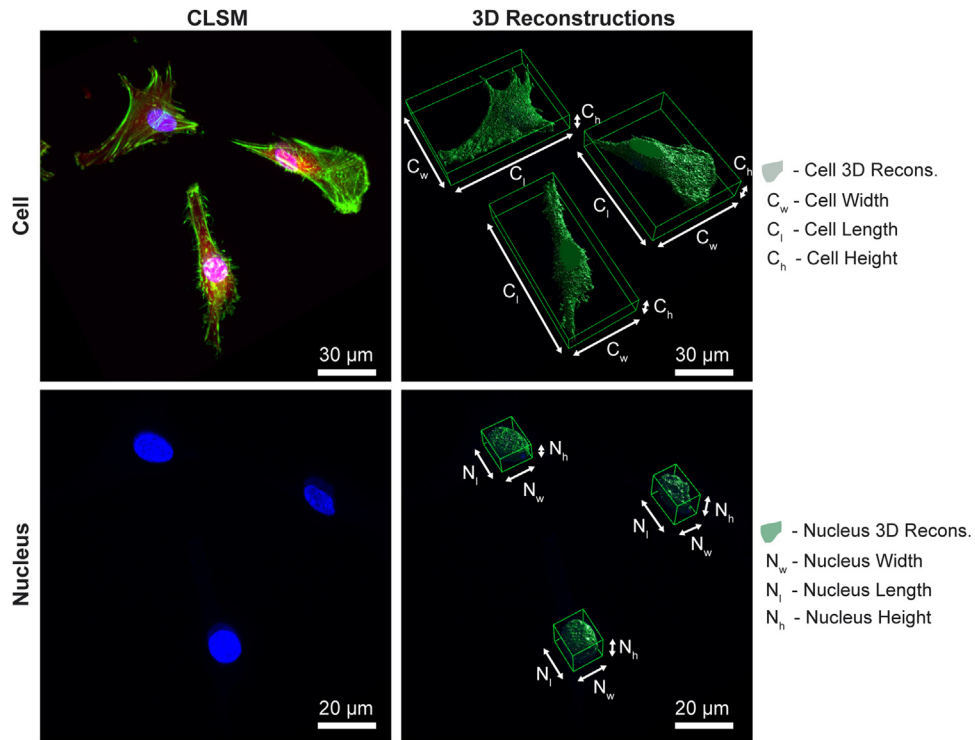
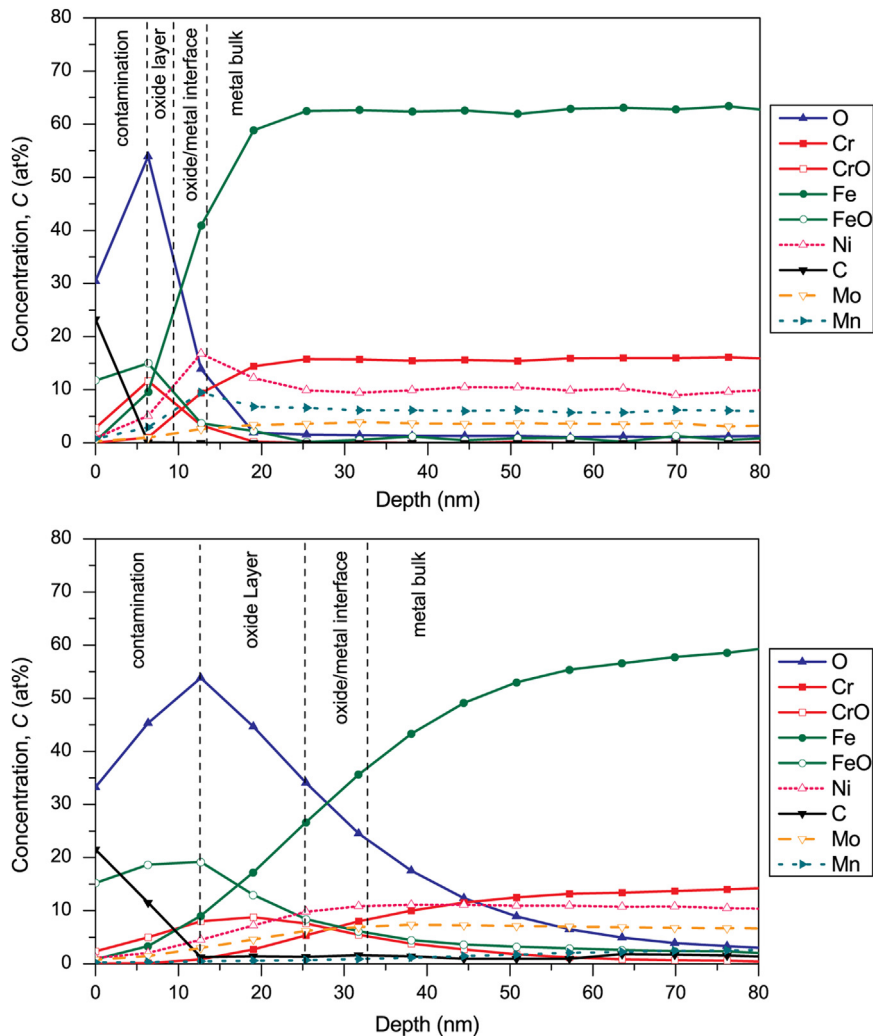


Fig. A.1 – CLSM images showing how the cell orientation was obtained.



**Fig. A.2** – CLSM micrographs (left) and 3D reconstructions (right) showing cells and nuclei on polished surfaces. FTIC-phalloidin (green), DAPI (blue) and HCS cell mask (deep red) respectively were used to stain the actin cytoskeleton, nuclei and cytoplasm. (For interpretation of the references to color in this figure legend, the reader is referred to the web version of this article.)



**Fig. A.3** – XPS depth profiles for (a) polished and (b) laser-ablated (LT-22) surfaces.

## REFERENCES

- Alberts, B., Johnson, A., Lewis, J., Raff, M., Roberts, K., Walter, P., 2002. *Molecular Biology of the Cell*, fifth ed. Garland Science, New York Classic textbook.
- Anselme, K., Bigerelle, M., 2005. Topography effects of pure titanium substrates on human osteoblast long-term adhesion. *Acta Biomater.* 1 (2), 211–222.
- Anselme, K., Bigerelle, M., Noël, B., Iost, A., Hardouin, P., 2002. Effect of grooved titanium substratum on human osteoblastic cell growth. *J. Biomed. Mater. Res.* 60 (4), 529–540.
- Belaud, V., Valette, S., Stremmsdoerfer, G., Bigerelle, M., Benayoun, S., 2015. Wettability versus roughness: multi-scales approach. *Tribol. Int.* 82, 343–349.
- Bershadsky, A., Kozlov, M., Geiger, B., 2006. Adhesion-mediated mechanosensitivity: a time to experiment, and a time to theorize. *Curr. Opin. Cell. Biol.* 18 (5), 472–481.
- Bigerelle, M., Anselme, K., Dufresne, E., Hardouin, P., Iost, A., 2002. An unscaled parameter to measure the order of surfaces: a new surface elaboration to increase cells adhesion. *Biomol. Eng.* 19 (2–6), 79–83.
- Biggs, M.J.P., Richards, R.G., Gadegaard, N., Wilkinson, C.D.W., Dalby, M.J., 2007. Regulation of implant surface cell adhesion: characterization and quantification of S-phase primary osteoblast adhesions on biomimetic nanoscale substrates. *J. Orthop. Res.* 25 (2), 273–282.
- Biggs, M.J.P., Richards, R.G., Gadegaard, N., Wilkinson, C.D.W., Oreffo, R.O.C., Dalby, M.J., 2009. The use of nanoscale topography to modulate the dynamics of adhesion formation in primary osteoblasts and ERK/MAPK signalling in STRO-1+ enriched skeletal stem cells. *Biomaterials* 30 (28), 5094–5103.
- Biggs, M.J.P., Richards, R.G., McFarlane, S., Wilkinson, C.D.W., Oreffo, R.O.C., Dalby, M.J., 2008a. Adhesion formation of primary human osteoblasts and the functional response of mesenchymal stem cells to 330 nm deep microgrooves. *J. R. Soc. Interface* 5 (27), 1231–1242.
- Biggs, M.J.P., Richards, R.G., Wilkinson, C.D.W., Dalby, M.J., 2008b. Focal adhesion interactions with topographical structures: a novel method for immuno-SEM labelling of focal adhesions in S-phase cells. *J. Microsc.* 231 (1), 28–37.
- Bruinink, A., Wintermantel, E., 2001. Grooves affect primary bone marrow but not osteoblastic MC3T3-E1 cell cultures. *Biomaterials* 22 (18), 2465–2473.
- Cao, Y., Chen, J., Adeoye, M.O., Soboyejo, W.O., 2009. Investigation of the spreading and adhesion of human osteosarcoma cells on smooth and micro-grooved polydimethylsiloxane surfaces. *Mater. Sci. Eng. C – Biomim. Supramol. Syst.* 29 (1), 119–125.
- Chehrودي, B., Gould, T.R.L., Brunette, D.M., 1992. The role of connective-tissue in inhibiting epithelial downgrowth on titanium-coated percutaneous implants. *J. Biomed. Mater. Res.* 26 (4), 493–515.
- Chen, J., Mwenifumbo, S., Langhammer, C., McGovern, J.P., Li, M., Beyre, A., Soboyejo, W.O., 2007. Cell/surface interactions and adhesion on Ti-6Al-4V: effects of surface texture. *J. Biomed. Mater. Res. Part B – Appl. Biomater.* 82B (2), 360–373.
- Chen, J., Ulerich, J., Abelev, E., Fasasi, A., Arnold, C., Soboyejo, W., 2009. An investigation of the initial attachment and orientation of osteoblast-like cells on laser grooved Ti-6Al-4V surfaces. *Mater. Sci. Eng.: C* 29 (4), 1442–1452.
- Clark, P., Connolly, P., Curtis, A.S.G., Dow, J.A.T., Wilkinson, C.D.W., 1990. Topographical control of cell behaviour: II. multiple grooved substrata. *Development* 108 (4), 635–644.
- Curtis, A., Wilkinson, C., 1997. Topographical control of cells. *Biomaterials* 18 (24), 1573–1583.
- Davidson, P., Bigerelle, M., Bounichane, B., Giazzon, M., Anselme, K., 2010. Definition of a simple statistical parameter for the quantification of orientation in two dimensions: application to cells on grooves of nanometric depths. *Acta Biomater.* 6 (7), 2590–2598.
- Davidson, P.M., Bigerelle, M., Reiter, G., Anselme, K., 2015. Different surface sensing of the cell body and nucleus in healthy primary cells and in a cancerous cell line on nanogrooves. *Biointerphases* 10 (3), 031004.
- den Braber, E.T., de Ruijter, J.E., Smits, H.T.J., Ginsel, L.A., von Recum, A.F., Jansen, J.A., 1996. Quantitative analysis of cell proliferation and orientation on substrata with uniform parallel surface micro-grooves. *Biomaterials* 17 (11), 1093–1099.
- Duncan, A.C., Weisbuch, F., Rouais, F., Lazare, S., Baquay, C., 2002. Laser microfabricated model surfaces for controlled cell growth. *Biosens. Bioelectron.* 17 (5), 413–426.
- Erdoğan, M., Öktem, B., Kalaycıoğlu, H., Yavaş, S., Mukhopadhyay, P.K., Eken, K., Özgören, K., Aykaç, Y., Tazebay, U.H., Ilday, F.Ö., 2011. Texturing of titanium (Ti6Al4V) medical implant surfaces with MHz-repetition-rate femtosecond and picosecond Yb-doped fiber lasers. *Opt. express* 19 (11), 10986–10996.
- Fischer, G., Bigerelle, M., Kubiak, K., Mathia, T., Khatir, Z., Anselme, K., 2014. Wetting of anisotropic sinusoidal surfaces – experimental and numerical study of directional spreading. *Surf. Topogr.: Metrol. Prop.* 2 (4), 044003.
- Gallant, N.D., 2013. 3 – Quantitative assays for measuring cell adhesion and motility in biomaterials. In: Jaffe, M., Hammond, W., Toliás, P., Arinze, T. (Eds.), *Characterization of Biomaterials*. Woodhead Publishing, Oxford, Cambridge, Philadelphia, New Delhi, pp. 72–100.
- Garcia, A.J., Gallant, N.D., 2003. Stick and grip – measurement systems and quantitative analyses of integrin-mediated cell adhesion strength. *Cell Biochem. Biophys.* 39 (1), 61–73.
- Gerecht, S., Bettinger, C.J., Zhang, Z., Borenstein, J.T., Vunjak-Novakovic, G., Langer, R., 2007. The effect of actin disrupting agents on contact guidance of human embryonic stem cells. *Biomaterials* 28 (28), 4068–4077.
- Holthaus, M.G., Stolle, J., Treccani, L., Rezwan, K., 2012. Orientation of human osteoblasts on hydroxyapatite-based microchannels. *Acta Biomater.* 8 (1), 394–403.
- Ismail, F.S.M., Rohanizadeh, R., Atwa, S., Mason, R.S., Ruys, A.J., Martin, P.J., Bendavid, A., 2007. The influence of surface chemistry and topography on the contact guidance of MG63 osteoblast cells. *J. Mater. Sci.: Mater. Med.* 18 (5), 705–714.
- Jayaraman, M., Meyer, U., Buhner, M., Joos, U., Wiesmann, H.P., 2004. Influence of titanium surfaces on attachment of osteoblast-like cells in vitro. *Biomaterials* 25 (4), 625–631.
- Jiang, L., Lu, X., Leng, Y., Qu, S., Feng, B., Weng, J., Watari, F., 2012. Osteoblast behavior on TiO<sub>2</sub> microgrooves prepared by soft-lithography and sol-gel methods. *Mater. Sci. Eng.: C* 32 (4), 742–748.
- Kenar, H., Köse, G.T., Hasirci, V., 2006. Tissue engineering of bone on micropatterned biodegradable polyester films. *Biomaterials* 27 (6), 885–895.
- Khang, D., Lu, J., Yao, C., Haberstroh, K.M., Webster, T.J., 2008. The role of nanometer and sub-micron surface features on vascular and bone cell adhesion on titanium. *Biomaterials* 29 (8), 970–983.
- Koutsopoulos, S., Patzsch, K., Bosker, W.T.E., Norde, W., 2007. Adsorption of Trypsin on hydrophilic and hydrophobic surfaces. *Langmuir* 23 (4), 2000–2006.
- Kubiak, K.J., Mathia, T.G., 2014. Anisotropic wetting of hydrophobic and hydrophilic surfaces – modelling by Lattice Boltzmann method. In: *Proceedings of the 37th National Conference on Theoretical and Applied Mechanics (37th NCTAM 2013)*. In: 1st International Conference on Mechanics (1st ICM), vol. 79. pp. 45–48.
- Kurella, A., Dahotre, N.B., 2005. Review paper: surface modification for bioimplants: the role of laser surface engineering. *J. Biomater. Appl.* 20 (1), 5–50.

- Lawrence, J., Hao, L., Chew, H.R., 2006. On the correlation between Nd:YAG laser-induced wettability characteristics modification and osteoblast cell bioactivity on a titanium alloy. *Surf. Coatings Technol.* 200 (18–19), 5581–5589.
- Lee, M.-H., Oh, N., Lee, S.-W., Leesungbok, R., Kim, S.-E., Yun, Y.-P., Kang, J.-H., 2010. Factors influencing osteoblast maturation on microgrooved titanium substrata. *Biomaterials* 31 (14), 3804–3815.
- Liu, X., Lim, J.Y., Donahue, H.J., Dhurjati, R., Mastro, A.M., Vogler, E.A., 2007. Influence of substratum surface chemistry/energy and topography on the human fetal osteoblastic cell line hFOB 1.19: phenotypic and genotypic responses observed in vitro. *Biomaterials* 28 (31), 4535–4550.
- Ma, C., Bai, S., Peng, X., Meng, Y., 2013. Anisotropic wettability of laser micro-grooved SiC surfaces. *Appl. Surf. Sci.* 284, 930–935.
- Malheiro, V.N., Spear, R.L., Brooks, R.A., Markaki, A.E., 2011. Osteoblast and monocyte responses to 444 ferritic stainless steel intended for a magneto-mechanically actuated fibrous scaffold. *Biomaterials* 32 (29), 6883–6892.
- Mata, A., Kim, E.J., Boehm, C.A., Fleischman, A.J., Muschler, G.F., Roy, S., 2009. A three-dimensional scaffold with precise micro-architecture and surface micro-textures. *Biomaterials* 30 (27), 4610–4617.
- Matsuzaka, K., Walboomers, X.F., de Ruijter, J.E., Jansen, J.A., 1999. The effect of poly-L-lactic acid with parallel surface micro groove on osteoblast-like cells in vitro. *Biomaterials* 20 (14), 1293–1301.
- McClay, D.R., Wessel, G.M., Marchase, R.B., 1981. Intercellular recognition: quantitation of initial binding events. *Proc. Natl. Acad. Sci. USA* 78 (8), 4975–4979.
- McGee, M.A., Howie, D.W., Costi, K., Haynes, D.R., Wildenauer, C. I., Percy, M.J., McLean, J.D., 2000. Implant retrieval studies of the wear and loosening of prosthetic joints: a review. *Wear* 241 (2), 158–165.
- O'Neill, W., Kun, L., 2009. High-quality micromachining of Silicon at 1064 nm using a high-brightness MOPA-Based 20-W Yb fiber laser. *IEEE J. Sel. Top. Quantum Electron.* 15 (2), 462–470.
- Perizzolo, D., Lacefield, W.R., Brunette, D.M., 2001. Interaction between topography and coating in the formation of bone nodules in culture for hydroxyapatite- and titanium-coated micromachined surfaces. *J. Biomed. Mater. Res.* 56 (4), 494–503.
- Qin, L., Zeng, Q., Wang, W., Zhang, Y., Dong, G., 2014. Response of MC3T3-E1 osteoblast cells to the microenvironment produced on Co–Cr–Mo alloy using laser surface texturing. *J. Mater. Sci.* 49 (6), 2662–2671.
- Reyes, C.D., García, A.J., 2003. A centrifugation cell adhesion assay for high-throughput screening of biomaterial surfaces. *J. Biomed. Mater. Res. Part A* 67 (1), 328–333.
- Robinson, H.J., Markaki, A.E., Collier, C.A., Clyne, T.W., 2011. Cell adhesion to plasma electrolytic oxidation (PEO) titania coatings, assessed using a centrifuging technique. *J. Mech. Behav. Biomed. Mater.* 4 (8), 2103–2112.
- Wang, P.-Y., Yu, H.-T., Tsai, W.-B., 2010. Modulation of alignment and differentiation of skeletal myoblasts by submicron ridges/grooves surface structure. *Biotechnol. Bioeng.* 106 (2), 285–294.
- Wang, X.F., Ohlin, C.A., Lu, Q.H., Hu, J., 2008. Cell directional migration and oriented division on three-dimensional laser-induced periodic surface structures on polystyrene. *Biomaterials* 29 (13), 2049–2059.
- Zhao, Y., Lu, Q., Li, M., Li, X., 2007. Anisotropic wetting characteristics on submicrometer-scale periodic grooved surface. *Langmuir* 23 (11), 6212–6217.
- Zheng, Y., Xiong, C., Wang, Z., Li, X., Zhang, L., 2015. A combination of CO<sub>2</sub> laser and plasma surface modification of poly(etheretherketone) to enhance osteoblast response. *Appl. Surf. Sci.* 344, 79–88.